Journal of
Micro/Nanolithography,
MEMS, and MOEMS

Nanolithography.SPIEDigitalLibrary.org

Chemoepitaxial guiding underlayers for density asymmetric and energetically asymmetric diblock copolymers

Benjamin D. Nation
Peter J. Ludovice
Clifford L. Henderson

SPIE.

Benjamin D. Nation, Peter J. Ludovice, Clifford L. Henderson, "Chemoepitaxial guiding underlayers for density asymmetric and energetically asymmetric diblock copolymers," *J. Micro/Nanolith. MEMS MOEMS* **16**(4), 043505 (2017), doi: 10.1117/1.JMM.16.4.043505.

Chemoepitaxial guiding underlayers for density asymmetric and energetically asymmetric diblock copolymers

Benjamin D. Nation,[a] Peter J. Ludovice,[a] and Clifford L. Henderson[a,b,c,*]
[a]Georgia Institute of Technology, Department of Chemical and Biomolecular Engineering, Atlanta, Georgia, United States
[b]Georgia Institute of Technology, Department of Chemistry and Biochemistry, Atlanta, Georgia, United States
[c]University of South Florida, Department of Chemical and Biomedical Engineering, Tampa, Florida, United States

Abstract. Currently, high χ block copolymers (BCPs) are being investigated as a method to extend optical lithography due to their ability to microphase separate on small size scales. Typically, BCPs with larger Flory–Huggin's χ parameters are composed of more dissimilar homopolymers. However, having dissimilar blocks changes how BCPs interact with their guiding underlayers. Several BCPs are simulated annealing on chemoepitaxial guiding underlayers using a coarse-grained molecular dynamics model to explore the effect that either energetic asymmetry or density asymmetry in the BCP have on the pattern registration. It is found that in varying the background region composition four regimes can be found. Minor variations in pinning stripe width are shown to have little effect on the window where well-aligned vertical lamellae form. For BCPs without an energetic mismatch, incommensurate films have the largest window for well-aligned vertical lamellae. However, with an energetic mismatch, the defectivity has a more complicated dependence on film thickness. Two different mixed lamellae (ML) morphologies can form depending on the film volume fraction and the relative compressibilities of the two blocks. It is found that more preferential background regions can be used when the BCP is transitioning between the two ML morphologies. This transition volume fraction shifts for a density asymmetric BCP, likely due to a difference in compressibilities of the two blocks. [DOI: 10.1117/1.JMM.16.4.043505]

Keywords: directed self-assembly; block copolymer; simulation; chemoepitaxy; molecular dynamics; process window.

Paper 17060SSP received Apr. 30, 2017; accepted for publication Nov. 6, 2017; published online Nov. 22, 2017.

1 Introduction

Currently, block copolymer-directed self-assembly (BCP-DSA) is a process being investigated as a method to supplement optical lithography in the making of smaller features in the microelectronics industry. BCPs are chemicals composed of two or more homopolymer (HP) blocks that are covalently bonded together. Typically, HPs do not mix well if there is a positive enthalpy of mixing between the two, denoted by the Flory–Huggins χ parameter. However, in a BCP these two HPs are covalently bonded, so the system cannot separate into two distinct bulk phases. Instead, the two blocks microphase separate to form regular repeating features on the scale size of the polymer chains themselves. The size of these features scales according to $L_0 \propto N^{\alpha} \cdot \chi^{\frac{1}{6}}$, where L_0 is the pitch or repeat distance of the features and N is the degree of polymerization of the BCP. In this equation, $\alpha = \frac{2}{3}$ in the strong segregation regime when the product of the Flory–Huggins χ parameter and the N is large while $\alpha = \frac{1}{2}$ in weak segregation regime (when χN is small).[1] Therefore, since the pitch is more strongly dependent on N, to decrease the pitch N should be made as small as possible. It has been found that for a BCP with a volume fraction of the A domain of $\phi_A = 0.5$, the phase separation will occur when $\chi N > 10.495$, and below this limit the BCPs will mix.[2,3] Therefore, to form smaller features, it is desired to find BCPs with as high a χ as possible to allow lower N BCPs to be used. BCPs tend to have higher χ values when the blocks interact in dissimilar ways, such as if one block primarily interacted through dispersion forces while the other had hydrogen bonding. There has been little modeling research done on BCPs that have density asymmetry or an energetic asymmetry.[4] The majority of modeling research to this point has been done investigating BCPs that are composed of two HPs that are identical to each other.[5,6] Therefore, little is known fundamentally about BCPs composed of blocks that interact in different ways and the effect that such energetic asymmetries has on phase separation or the ability to align BCP films to patterned underlayers. However, it is known to be important since energetically asymmetric BCPs are known to often "skin," preferentially placing the block with the lower cohesive energy density (CED) at the free surface.

To use BCPs in the microelectronics industry, a process known as DSA is used. In this process, optical lithography is used to make a guiding underlayer, which then directs the phase separation of a BCP film. These underlayers direct the BCP into useful patterns, which need to be defect free to be useful. One form of underlayer being explored is a chemoepitaxial guiding underlayer, where the guidance to the BCP film is performed using regions of differing chemical preference on the underlayer. An example of these underlayers for a lamellae forming diblock copolymer film is

*Address all correspondence to: Clifford L. Henderson, E-mail: clhenderson@usf.edu

1932-5150/2017/$25.00 © 2017 SPIE

an underlayer composed of a repeating pattern of a thin, highly preferential pinning stripe followed by a larger, more neutral background region. In this case, the pinning stripe will pin down one block of the BCP, and then the order will propagate across the background region. This is similar to the type of underlayer produced by the LiNe process flow.[7] Modeling research has been done in these underlayers, though only on BCPs that are symmetric in energy and density.[7–9] This paper seeks to explore what problems might be encountered in the future when using more asymmetric, high χ BCPs. This research is done using a coarse-grained molecular dynamics model.

2 Model Description

This work is performed using a coarse-grained molecular dynamics model developed elsewhere.[5,10] Polymers are coarse grained such that four monomeric units are combined into one unified atom or bead. This level of coarse graining was chosen to be beyond the statistical segment length of many common polymers used in BCPs, such as poly(styrene) and poly(methyl methacrylate). Beads are connected to each other using a harmonic bond potential of the form

$$V_{\text{bond}} = \frac{1}{2} \cdot k_{\text{bond}} \cdot (r_{\text{eq}} - r)^2, \tag{1}$$

where V_{bond} is the harmonic bond potential, k_{bond} is the bond force constant, r_{eq} is the equilibrium bond length, and r is the measured length of the bond. For all forcefields in this paper, $k_{\text{bond}} = 100(\frac{\text{kcal}}{\text{mol}})$ and $r_{\text{eq}} = 0.82$ nm.

Every three consecutively bonded beads has a harmonic angle potential acting on them of the form

$$V_{\text{angle}} = \frac{1}{2} \cdot k_{\text{angle}} \cdot (\theta_{\text{eq}} - \theta)^2, \tag{2}$$

where V_{angle} is the harmonic angle potential, k_{angle} is the angle force constant, θ_{eq} is the equilibrium angle between the three beads, and θ is the measured angle. For all forcefields in this paper, $k_{\text{angle}} = 5(\frac{\text{kcal}}{\text{mol}})$ and $\theta_{\text{eq}} = \frac{2}{3} \cdot \pi$.

A nonbonded potential is present between every pair of beads that are not bonded or participating in the same angle potential. The form of the nonbonded potential is

$$V_{ij}(r) = \varepsilon_{ij} \cdot \left[\left(\frac{\sigma_{ij}}{r} \right)^8 - 2 \cdot \left(\frac{\sigma_{ij}}{r} \right)^4 \right], \tag{3}$$

where V_{ij} is the nonbonded potential between beads of type i and j, ε_{ij} is the strength of the nonbonded interaction, σ_{ij} is the radius of the minimum energy, and r is the distance between two beads. The value of the nonbonded potential is zero when beyond a cut-off radius of $R = 4$ nm.

The parameters ε_{ij} and σ_{ij} have large effects on CED and density (ρ), respectively. Therefore, these values were varied to generate three different HPs, which are summarized in Table 1. The first HP, HP 1, is the HP typically used in this model. This HP is meant to be roughly equivalent to polystyrene. The second HP described in Table 1 was designed to have a similar density to HP 1 but a different CED. The third HP was designed to have a similar CED to HP 1 but a different density.

Table 1 Summary of the forcefields for each HP and some resulting properties.

HP	σ_{AA} (nm)	ε_{AA} $\left(\frac{\text{kcal}}{\text{mol}}\right)$	CED $\left(\frac{\text{kcal}}{\text{mol}}\right)$	ρ $\left(\frac{\text{beads}}{\text{nm}^3}\right)$	β (MPa^{-1})
1	1.26	0.500	12.95	1.37	408
2	1.30	0.537	15.26	1.37	377
3	1.17	0.480	13.20	1.55	469

These HPs were then used to create five diblock copolymers (BCPs), which are summarized in Table 2. The symmetric BCP is a BCP where each block is the same HP 1. This is an idealized case where the density and cohesive energy densities of both blocks are identical. Most simulation work to this point has considered idealized BCPs such as this.[5,6] It should be noted that while the cohesion of HP A with itself is the same as the cohesion of HP B with itself, by altering ε_{AB} there can still be a value of χ present since the cohesion of A with B is lessened. This would be similar to having two blocks that have equivalent cohesive energy densities, but having one block interacts primarily through dispersion forces while the other interacts primarily through polar forces or hydrogen bonding.

The next two BCPs are formed using HP 1 and HP 2, which have a CED mismatch. The CED ratio here is in the range of many BCPs, though relatively small in comparison to some high χ BCPs. However, this allows the BCP to be simulated without needing to add a topcoat, which greatly simplifies the system.

The final two BCPs are formed using HP 1 and HP 3, which have a density mismatch. The density mismatch is similar to that found between polystyrene and poly(methyl methacrylate). There is also a small difference in the CED of these two HPs. However, since the CED ratio (1.02) is very close to one, it is assumed that the trends observed for these BCPs will be primarily due to the larger difference in densities, which have a ratio of 1.13.

All BCPs were made using a degree of polymerization (N) of 64 monomers (16 beads). Typically, each block of the BCP has a degree of polymerization of 32 monomers (eight beads). However, Secs. 3.5 and 3.6 both include polymers with varying volume fraction. In these cases, the

Table 2 Summary of nonbonded potential parameters for various forcefields and resulting properties.

BCP	HP A	HP B	σ_{AB} (nm)	ε_{AB} $\left(\frac{\text{kcal}}{\text{mol}}\right)$	L_0 (nm)	$\frac{\text{CED}_A}{\text{CED}_B}$	$\frac{\rho_A}{\rho_B}$
Symmetric	HP 1	HP 1	1.26	0.325	12.41	1.00	1.00
$\text{CED}_A < \text{CED}_B$	HP 1	HP 2	1.28	0.345	12.43	0.85	1.00
$\text{CED}_A > \text{CED}_B$	HP 2	HP 1	1.28	0.345	12.43	1.18	1.00
$\rho_A < \rho_B$	HP 1	HP 3	1.21	0.272	12.83	0.98	0.88
$\rho_A > \rho_B$	HP 3	HP 1	1.21	0.272	12.83	1.02	1.13

minority block has 28 monomers (seven beads), and the majority block has 36 monomers (nine beads). The mass of each bead in the system is 418.4 Da.

The value of ε_{AB} was chosen for all BCPs in Table 2 such that χ has a value of 0.78 and χN has a value of 50. While this value of χ is high in comparison to many BCPs in use now,[11] it allows for a smaller degree of polymerization while still maintaining a reasonable value of χN. This makes the simulated BCP have a smaller domain size, which in turn allows for smaller simulation volumes and quicker simulation run times. While having a higher χ, lower N will likely alter the absolute defectivity, there should be little effect on the relative defectivity within a series as is discussed in this work.

Simulations are built using custom code written in MATLAB.[12] Molecular dynamics was run using HOOMD-blue on a graphics processing unit cluster.[13,14] Simulation results were viewed using code written in MATLAB.

The underlayers in this work are brush underlayers, where each brush is a seven bead chain ($N = 28$) that has one end fixed in space. The brush chains were placed on a square lattice in the horizontal plane with an areal brush density of 0.44 brushes/nm^2, or with a node spacing of 1.5 nm. To simulate a hard surface underneath the brush that the brush is grafted to and prevent chain inversion, a second layer of fixed beads was added.[5] These beads were placed on a lattice located between the lattice points of the upper layer but at a distance 0.83 nm below the first layer. The brush is a random copolymer of the two bead types composing the BCP being simulated. To simulate a chemoepitaxial guiding underlayer, a pinning stripe is patterned into the brush underlayer by making all the beads in a particular region bead type A ($n_{A,\text{pinning}} = 1$). Unless otherwise mentioned, the width of the pinning stripe is $0.5 \cdot L_0$. Separating pinning stripes is a background region in which beads are assigned randomly between types A and B such that the overall number fraction ($n_{A,\text{background}}$) of the background region is at some set value, which is varied in this paper. The background region is always sized so that the overall pattern pitch is $W_{\text{pattern}} = W_{\text{pinning}} + W_{\text{background}} = 2 \cdot L_0$, making the pattern a density doubling pattern.

To make the BCP films, BCP chains are generated using a random walk and placed randomly within a box that has the dimensions of the desired film until the appropriate density is reached. Next, the BCP chains are wrapped periodically in the x and y dimensions. Finally, the film is placed on top of the desired underlayer. These films are initially well mixed. All simulations were built with x and y dimensions of $6 \cdot L_0 \times 6 \cdot L_0$, where L_0 is the pitch of the BCP as reported in Table 2. In general, films are built at $0.5 \cdot L_0$ thickness, though in some sections $0.75 \cdot L_0$ and $1.0 \cdot L_0$ are also used. The thinner film thicknesses are valuable since these films have a quicker run time than thicker films.

Once built, simulations undergo two minimization steps. The first minimization has the purpose of gently pushing apart any beads that are initially placed too close together. This is done by initially setting the value of all σ_{ij} to a very low value. This decreases the radius of the highly repulsive regime of the nonbonded potential. A short 50 timestep minimization is run using the HOOMD FIRE minimizer (parameters: $d_t = 5 \times 10^{-6}$, $f_{\text{tol}} = 1 \times 10^{-2}$, $E_{\text{tol}} = 1 \times 10^{-7}$, $f_{\text{inc}} = 1.99$, $f_{\text{dec}} = 0.8$, alpha_start $= 0.01$, and $f_{\text{alpha}} = 0.9$). Once complete, the value of σ_{ij} is increased and the process is repeated until the desired values of σ_{ij} are reached.

Next, a second minimization step is run. This minimization runs for 20,000 timesteps using the FIRE minimizer with parameters $d_t = 5 \times 10^{-4}$, $f_{\text{tol}} = 1 \times 10^{-2}$, and $E_{\text{tol}} = 1 \times 10^{-7}$. Once both minimization steps are complete, the full simulations are run using the HOOMD constant number of particles, volume, and temperature integrator (Nose–Hoover thermostat with temperature set point of $T = 500$ K and a controller coupling constant of $\tau = 0.2$ timesteps) with a timestep of 0.05 ps. Simulations are run in two stages. First, the films are run 10 ns (200,000 timesteps) with $\varepsilon_{AB} = \frac{1}{2} \cdot (\varepsilon_{AA} + \varepsilon_{BB})$ (where $\chi = 0$) to relax out any unrealistic density fluctuations from the initial build. Second, simulations are run 100 ns (2,000,000 timesteps) with the appropriate ε_{AB} or χ allowing phase separation to occur. Nine replicates are run for each simulation in this work.

To determine the defectivity of a film after an MD simulation, a top-down projection of the simulation was produced. This was done by forming a grid of pixels spaced 0.3 nm apart and coloring each pixel based on the number fraction of A beads in the film within a radius of 1 nm. Next, contour lines were generated along the number fraction of 0.5 to trace the interface between the A and B domain. For well-formed lamellae, these contours should all approximately be in the same direction except for some variation due to line edge roughness. Therefore, any contour that had an angle deviating from the desired angle by $\frac{\pi}{6}$ was noted to be potentially defective. Any pixel that had >10 of these potentially defective contour line segments within a $\frac{1}{3} \cdot L_0$ radius was labeled as defective. After doing this, the defective area fraction was calculated. This defect area fraction was averaged over the nine replicates and called the defectivity. The defectivity ranged from 1 (totally defective films) to 0 (defect free, well-aligned vertical lamellae).

This measure of defectivity is a kinetic snapshot of the defectivity, not an equilibrium measure of defectivity. With more simulated thermal annealing time, the defectivity can continue to decrease. This is particularly true if the defectivity is due to line defects. On the other hand, a defectivity due to morphological defects tends to not decrease. This kinetic snapshot of the defectivity is a valuable measurement since many defects present in BCPs experimentally are hypothesized to be kinetically trapped. Additionally, it is likely that this kinetic snapshot of defectivity should be correlated with the equilibrium defectivity.

3 Results and Discussion

3.1 *Defectivity Versus Background Region Composition*

Simulations were run for a symmetric BCP of thickness $0.5 \cdot L_0$ on a patterned underlayer with an A pinning stripe ($n_{A,\text{pinning}} = 1$). The composition of the background region of the underlayer, $n_{A,\text{background}}$, was varied and the defectivity of the resulting film was measured. These data are shown in Fig. 1. Four different regimes are observed in this data as will be described below. The general shape of the curve in Fig. 1 and the four regimes/morphologies described here are seen in all of the following series of simulations.

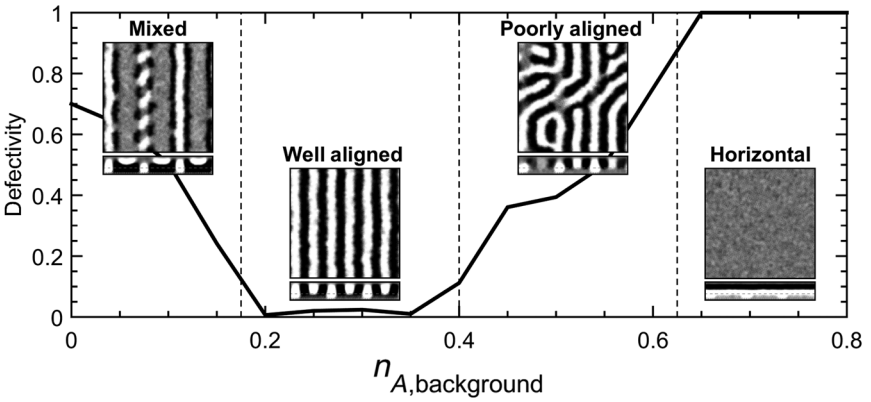

Fig. 1 The measured defectivity for a symmetric BCP film of thickness $0.5 \cdot L_0$ on a series of underlayers with $n_{A,\text{pinning}} = 1$ and a varying $n_{A,\text{background}}$. Four different regimes of film morphology are observed, an ML morphology at low $n_{A,\text{background}}$, a well-aligned vertical lamellae morphology, a poorly aligned vertical lamellae morphology, and a horizontal lamellae morphology. Examples of these four morphologies are shown in the inset images, with the top image being a top-down view and the bottom being a cross-sectional view. The dashed gray line in the cross-sectional view indicates the approximate interface of the brush underlayer and the film.

First, at high background composition, $n_{A,\text{background}} \to 1$, the BCP film is in a regime where it forms a horizontal lamellae morphology. In this regime, the underlayer is predominately A beads since the composition of the pinning stripe is also $n_{A,\text{pinning}} = 1$. Therefore, the film forms horizontal lamellae sheets with the A block wetting the underlayer. Within this regime, the defectivity typically has a value of 1.

As the background region composition is decreased, eventually a point is reached, where vertical lamellae can form. However, since there is very little contrast between the pinning stripe ($n_{A,\text{pinning}} = 1$) and the background region, the underlayer gives very little guidance to the film. Therefore, instead of forming well-aligned lamellae, the resulting film is more reminiscent of a fingerprint pattern. For this reason, this regime is referred to as poorly aligned vertical lamellae. Defectivity in this region is very high at high background region compositions but decreases as $n_{A,\text{background}}$ decreases. This decrease is due to an increase in the contrast in the background region and the pinning stripe. Having a high contrast between the background region and the pinning stripe causes there to be a high energetic penalty for the wrong type lamellae to be over the wrong region. For example, there is a high energetic penalty when a B type lamellae is above an A type pinning stripe. Eventually, there comes a point as $n_{A,\text{background}}$ decreases that there is enough contrast to essentially eliminate all defects. This is the well-aligned vertical lamellae regime and is ultimately the target in the underlayer design process.

However, moving past this where $n_{A,\text{background}} \to 0$ a final regime is entered where the film forms what is referred to here as mixed lamellae (ML) morphology. This morphology appears to be a mixture of two morphologies that have been presented in the literature,[6] specifically the vertical lamellae without asymmetry and B dot morphologies. An example of this phase is shown in Fig. 1. In this regime, the film is attempting to simultaneously form both horizontal lamellae with the B block wetting the underlayer above the background region and vertical lamellae near the pinning stripe. The driving force for the formation of the horizontal lamellae is the highly preferential background region, whereas the driving force for the vertical lamellae is the high contrast between the background region and the pinning stripe. This contrast offers very strong guidance for BCP chains in the vicinity of the pinning stripe/background region interface, strong enough to counteract the predominate B underlayer.

It is helpful to categorize defects as one of the two types, line defects and morphological defects. Line defects are defects such as jogs or dislocation pairs that exist in vertical lamellae. These are the sorts of defects that exist in the well-aligned and poorly aligned vertical lamellae regimes. These line defects decrease with more guidance/contrast in the system, meaning they decrease as $n_{A,\text{background}}$ decreases. However, there also exist morphological defects. These are defects where the BCP is forming an incorrect morphology (e.g., mixed horizontal and vertical lamellae). These morphological defects occur at extreme values of $n_{A,\text{background}}$.

The most desirable background composition will be one that minimizes line defects while still preventing all morphological defects. This composition will be the lowest $n_{A,\text{background}}$ that still prevents the formation of the mixed horizontal and vertical lamellae morphology. This implies that one way to decrease defectivity is to destabilize the ML morphology. If the ML morphology is less stable, it will not form until even lower values of $n_{A,\text{background}}$. This allows lower values of $n_{A,\text{background}}$ to be reached while still forming vertical lamellae, further decreasing the number of line defects. In later sections, it will be suggested that this can be done by altering the film thickness or the volume fraction of the BCP.

3.2 *Pinning Stripe Width*

Simulations were run to calculate the defectivity versus background composition curves for five different pinning stripe widths for symmetric BCPs. The films were all $0.5 \cdot L_0$ thick and had a volume fraction of $\phi_A = 0.5$. These results are shown in Fig. 2. All pinning stripe widths measured here other than $W_{\text{pin}} = 0.62 \cdot L_0$ have very similar defectivity windows. However, the simulation series with a pinning stripe of $W_{\text{pin}} = 0.5 \cdot L_0$ may have a slightly larger

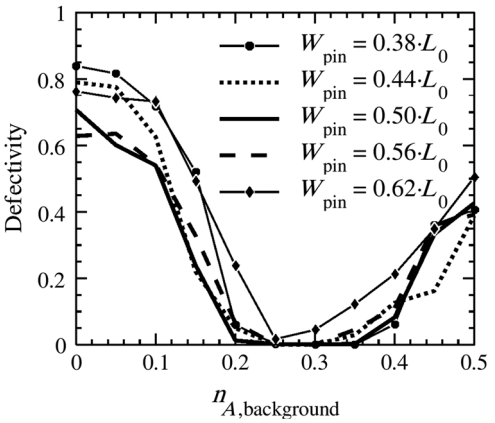

Fig. 2 Defectivity measurements for a five different pinning stripe widths (W_{pin}) while varying the background region composition ($n_{A,\text{background}}$). BCP films are symmetric in energy and density with a volume fraction $\phi_A = 0.5$.

window for well-aligned vertical lamellae than the other three. While this may be due to the width of the pinning stripe being commensurate with the width of one lamellae, the difference is ultimately very slight and likely within noise. On the other hand, when significantly oversizing the pinning stripe ($W_{\text{pin}} = 0.62 \cdot L_0$) the defectivity increased for all background compositions. Morphological defects appeared to occur at higher background compositions than in the other cases ($n_{A,\text{background}} = 0.20$ instead of 0.15 for the others). Additionally, the vertical lamellae never got to as low a defectivity. However, this pinning stripe is fairly large (25% larger than the best case here of $W_{\text{pin}} = 0.5 \cdot L_0$). When only 12.5% oversized, the pinning stripe had little effect on the defectivity. This suggests that this process is fairly tolerant of variations in the pinning stripe.

3.3 *Film Thickness*

The effect of film thickness on the defectivity of a symmetric BCP film was explored. The results for three different film thicknesses, t, are shown in Fig. 3. First, it should be noted that it appears there is more noise and higher defectivity in the curves with increasing film thickness. This is likely due to the simulations all being run the same length of simulation time (100 ns) when thicker films typically require more simulation time on average to reach a stable state. Thicker films require more time for two main reasons. First, it takes longer for the influence of the underlayer to propagate through the thickness of the film. Second, and related to the first, since initially the films will phase separate before the tops of the film feel the effect of the underlayer, the top of the thick films is likely to initially form a more highly defective state. This defective state takes more time to anneal out, particularly since it is only indirectly influenced by the underlayer. While this makes it difficult to compare quantitatively between film thickness, one can still consider qualitative differences between the trends.

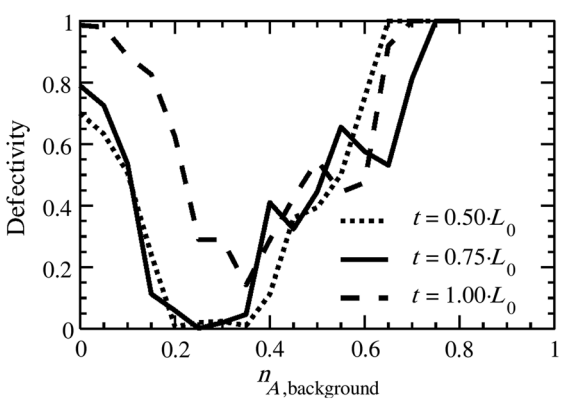

Fig. 3 Defectivity measurements for a symmetric BCP with three different film thicknesses t.

The window for forming well-aligned vertical lamellae is larger for $t = 0.75 \cdot L_0$ than $t = 1.00 \cdot L_0$. This can be explained by looking at the level of frustration in the two respective films. When a lamellae film is a thickness of $n/2 \cdot L_0$, where n is some integer, the film is considered not to be frustrated. This is because at these film thicknesses there exists a possible configuration where the chains pack at the appropriate density to form horizontal stacked lamellae without any islands and/or holes present. However, if the film is frustrated, such as in the $t = 0.75 \cdot L_0$ case, no such configuration exists, causing any horizontal lamellae morphology to consist of islands and/or holes. For a symmetric BCP, these islands and/or holes are unfavorable since they increase the interfacial area between the BCP film and the free surface. Increasing this interfacial area increases the free energy because beads at the free interface have fewer beads in close proximity, both because there is a slight decrease in density near the free interface and because there is a vacuum above these beads. This equates to the beads near the free interface participating in less attractive nonbonded potential pairs, increasing their enthalpy.

Looking only at the contribution of the free interface to the free energy of a symmetric BCP film, varying the film thickness should have no effect on the free energy of the vertical lamellae morphology. This is because the vertical lamellae morphology can form a flat surface at any film thickness. However, the film thickness has a large effect on the horizontal lamellae morphology since a commensurate film can form a flat surface while an incommensurate film must form islands and/or holes. Since the ML morphology has a horizontal lamellae component, it too will have a higher free energy when at an incommensurate film thickness. Because of this increase in the free energy of the ML morphology, a larger driving force to form ML must be present before the film enters that state. Therefore, having an incommensurate film thickness allows a more preferential background region, which in turn allows for lower line defectivity to be present.

The more interesting comparison in this data is between $t = 0.50 \cdot L_0$ and $t = 1.00 \cdot L_0$. Since both of these films have an equal level of frustration one would expect both films to behave similarly. However, while these two films behave in a similar manner at higher background compositions, at low background compositions $t = 0.50 \cdot L_0$ behaves more like the $t = 0.75 \cdot L_0$ case. The ML morphology is inherently a high-energy state. This morphology has more intrinsic BCP interfacial area than any other and, therefore, is resisted. With an increased film thickness, $t = 1.00 \cdot L_0$ is far better suited to disperse this energy than $t = 0.50 \cdot L_0$. Therefore, $t = 0.50 \cdot L_0$ resists forming the ML morphology until even lower background region compositions.

3.4 *Cohesive Energy Density Asymmetry*

A BCP that is asymmetric in CED is considered next. Simulations were run to determine the window for well-aligned vertical lamellae for three different film thicknesses. These results are shown in Fig. 4 for both cases, where $\mathrm{CED}_A > \mathrm{CED}_B$ and $\mathrm{CED}_A < \mathrm{CED}_B$ (where the pinning stripe is always A).

In both of these cases, film thickness plays a major role in the location of the well-aligned vertical lamellae window, as has been discussed previously for unpatterned underlayers.[4] This can largely be explained by considering the role the free surface now plays in DSA. With the symmetric BCP, neither block preferred the free surface since the CEDs of the two blocks matched. However, now that there is a mismatch in CED, the block that is lower in CED will preferentially go to the surface. As discussed earlier, beads at the free interface experience less attractive interactions with beads in the film. Because of this, there is a larger energetic penalty to place the higher CED block at the free surface since there will be a greater loss of attractive interactions than if the lower CED block were at the free surface. This effect causes the CED asymmetric BCP to skin if the CED ratio is high enough. The drive to skin has a large effect on what morphology forms at what background region composition.

A film of thickness $t = 0.5 \cdot L_0$ allows for three possible nonmixed lamellar configurations without islands or holes: vertical lamellae, horizontal lamellae with the A block down (denoted as AB), and horizontal lamellae with the B block down (BA). Looking at just the free interface, when $\mathrm{CED}_A > \mathrm{CED}_B$ the AB configuration will be the most stable morphology since it places the lower CED block at the free surface. To counteract this free interface driving force, the underlayer will need to be more preferential to B type beads (lower $n_{A,\mathrm{background}}$) to form vertical lamellae instead of the AB configuration. Therefore, for $\mathrm{CED}_A > \mathrm{CED}_B$ [Fig. 4(a)] the window for $t = 0.5 \cdot L_0$ will shift to the left. On the other hand, since $\mathrm{CED}_A < \mathrm{CED}_B$ [Fig. 4(b)] will have a more stable BA morphology, its window would have to shift to higher compositions (to the right).

In a similar way, with a film thickness of $1 \cdot L_0$ there are three possible nonmixed lamellar configurations without islands or holes: vertical lamellae, horizontal lamellae with A on both the top and bottom (denoted as $ABBA$), and horizontal lamellae with B on both the top and bottom ($BAAB$). In this case for $\mathrm{CED}_A > \mathrm{CED}_B$, the CED makes $BAAB$ the more stable configuration since it places the lower CED block at the free surface. Therefore, unlike the $t = 0.5 \cdot L_0$ case, the window will shift to a higher background composition.

Comparing between $\mathrm{CED}_A < \mathrm{CED}_B$ and $\mathrm{CED}_A > \mathrm{CED}_B$ for a film thickness of both $t = 0.75 \cdot L_0$ and $t = 1.00 \cdot L_0$, it can be seen that $\mathrm{CED}_A < \mathrm{CED}_B$ reaches far lower defectivities within its window. This is due to the window of $\mathrm{CED}_A < \mathrm{CED}_B$ being shifted to the left, where there is more contrast between the pinning stripe and background region. This supports the idea that line defects continue to decrease as more contrast is introduced into the system.

The fact that the low defectivity window shifts in opposite directions for films of thickness $n \cdot L_0$ and $(n + 1/2) \cdot L_0$ shows that with a CED asymmetric BCP, the stability of the ML morphology has a large dependence on film thickness. Therefore, with the proper choice of pinning stripe and film thickness, one can design an underlayer with far greater guidance while still forming vertical lamellae, thus eliminating more line defects. The ideal cases would be either a film with a higher CED pinning stripe and a film thickness of $(n + 1/2) \cdot L_0$ or a lower CED pinning stripe and a film thickness of $n \cdot L_0$.

3.5 *Volume Fraction Asymmetry*

The volume fraction of a symmetric BCP film was varied. Simulations were run with three film volume fractions, ϕ_A, for a $0.5 \cdot L_0$ thick film on an underlayer with a pinning stripe of $W_{\mathrm{pin}} = 0.5 \cdot L_0$. In Fig. 5, it can be seen that the volume fraction of the film has a fairly large effect on the defectivity profile. Shifting the volume fraction away from $\phi_A = 0.5$ causes the ML regime to extend to higher background compositions. Additionally, it is observed that the well-aligned vertical lamellae regime when $\phi_A = 0.4375$ extends to higher background compositions, and then when the defects start appearing, they appear at a slower rate.

It is hypothesized that having a volume fraction other than $\phi_A = 0.5$ increases the kinetics of defect annihilation. It has been shown that a key step in annealing out many common defects is the formation of a bridge of one domain across another.[15] When $\phi_A < 0.5$, the A lamellae will be narrower while the B lamellae will be wider. Related to this, the A portion of the chains will be shorter while the B portion of the chain will be longer. With these two facts in mind, there are two ways a volume fraction of $\phi_A < 0.5$ could

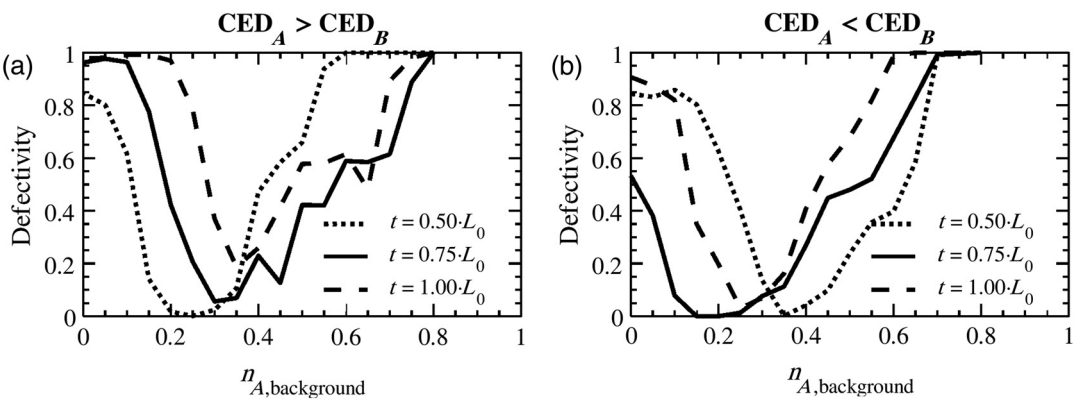

Fig. 4 Defectivity measurements of three different film thicknesses (t) for (a) a BCP with the CED of block A greater than block B and (b) a BCP with the CED of block A less than block B.

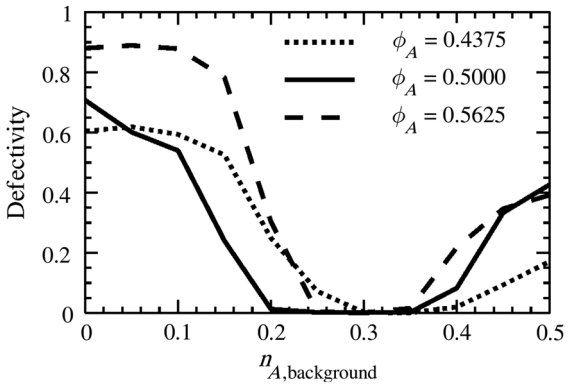

Fig. 5 Defectivity measurements for a BCP that is symmetric in energy and density, but with varying volume fraction ϕ_A for a film thickness of $t = 0.5 \cdot L_0$.

increase the bridge formation. First, the shorter A portion of a chain will be easier to drag through a B domain, though the B domain is wider, which may counteract the effect. Second, the longer B chain, while likely harder to drag through an A domain, does not have to be dragged as far since the A domain is narrower.

While it is out of the scope of this paper to work out all the intricacies of this situation, a brief proof of concept was tested. A proxy for bridge formation, and therefore the kinetics of defect annihilation, is a count of how many times a BCP chain, which is typically centered on a lamellar interface, jumps from one interface to an adjacent one. For a chain to jump interfaces, it is necessary for one portion of its chain to be dragged through an unfavorable domain (e.g., the A block must pass through the B domain). To measure this rate, defect-free thin film simulations were built. These films had dimensions of $2 \cdot L_0 \times 6 \cdot L_0 \times 0.5 \cdot L_0$ and were built on a 2× density multiplying underlayer with an A preferential pinning stripe and a background region of $n_{A,\text{background}} = 0.5$. Due to these chain jumps being rare, 50 replicates were run for 100 ns each. The positions were recorded every 5 ns, with the final 80 ns of the simulation being analyzed to see when the center of mass of a chain jumped from one interface to another. The results are shown in Table 3.

Table 3 Counts of chains jumping from one interface to another in thin film defect-free lamellae simulations. Columns N_A and N_B show the number of A and B beads per chain. Columns A (pin), A (back), and B indicate the number of chains jumping across the A domain above the pinning stripe, the A domain above the background region, and the two B domains above the background region.

ϕ_A	N_A	N_B	A (pin)	A (back)	B	Total
0.4375	7	9	4	0	17	21
0.5000	8	8	4	1	2	7
0.5625	9	7	10	9	0	19

It can be seen that the minority block is far more likely to cross over the majority domain. This supports the explanation that a shorter portion of a chain can jump easier despite it needing to jump a longer distance. Also, it shows that a volume fraction other than $\phi_A = 0.5$ does have increased jumping rates since $\phi_A = 0.5$ had approximately a third of the chain jumps that either of the other volume fractions had. This suggests bridge formation would likely be easier for these polymers. While this is not a perfect proxy for defect annihilation, it does suggest that defect annihilation may be improved by having a volume fraction other than $\phi_A = 0.5$. This is supported further by data in Sec. 3.6. However, it is unclear why the defectivity in the case of $\phi_A = 0.5625$ does not decrease as it did in $\phi_A = 0.4375$. This may be due to the presence of the pinning stripe, as it can be seen that chains appear more likely to jump across the A domain located above the pinning stripe rather than the A domain located above the background region.

The BCP film with a volume fraction of $\phi_A = 0.5$ forms well-aligned vertical lamellae at far lower background region compositions than the other two BCP films. This is due to each of these three BCP films forming a slightly different ML morphology, as shown in Fig. 6. These morphologies are seen when the underlayer is composed of a background region that is sufficiently preferential to B with an A preferential pinning stripe. While these morphologies do occur at

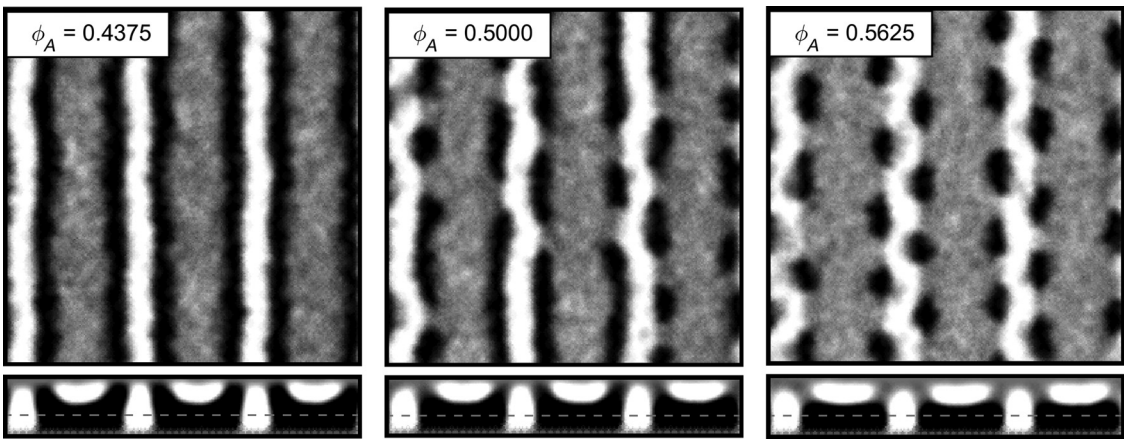

Fig. 6 Top-down and cross-sectional images of simulations for a symmetric BCP film of thickness $0.5 \cdot L_0$ with varying film volume fraction on an underlayer with $n_{A,\text{background}} = 0$ and $n_{A,\text{pinning}} = 1$. The A block is indicated by white, the B block by black, and the approximate interface between the film and the underlayer is indicated by the dashed gray line.

other background preferences, they are the clearest with the strong guidance of $n_{A,\text{background}} = 0$, the case as shown in Fig. 6. When the A block (white) is the minority block in the film ($\phi_A = 0.4375$), the ML morphology looks more lamellar. The vertical lamellae above the pinning stripe forms very well with a half lamellae of black on either side of the white lamellae. On the other hand, when the A block is the majority block ($\phi_A = 0.5625$), a different, more cylindrical morphology forms. Near the underlayer/film interface, there is good registration of the film with the underlayer pattern as in the earlier case. However, further from the underlayer interface instead of the B domain forming half lamellae, a more cylindrical shape is formed. This is at least in part due to B being the minority phase, so it can form the cylinders while the A phase forms the matrix around it. Interestingly, these cylinders appear to be roughly half cylinders, meaning they have more of a semicircular cross section. This is due to the chains that compose the cylinders being primarily contributed by the vertical lamellae portion of the film with little contribution from the horizontal region. Because the cylinders are only gaining mass from one side, there is effectively a lower local volume fraction of B in this area than there are for typical cylinders. This helps explain why a lamellae forming BCP with a volume fraction well inside the lamellae phase on a typical phase diagram[2] might have cylindrical components in its morphology. The placement of these B type half cylinders tends to be staggered across the vertical lamellae, causing the vertical lamellae to waver from side to side to accommodate. When the volume fraction of the film is $\phi_A = 0.5000$, the film seems to be transitioning between these two morphologies.

When $\phi_A = 0.4375$ the lamellar form is more stable, meaning it has a lower free energy, when $\phi_A = 0.5625$ the cylindrical form has a lower free energy. On the other hand, when $\phi_A = 0.5000$ it is suspected that the lamellar form and the cylindrical form have similar free energies leading to this hybrid state. More importantly, it is hypothesized that the free energy of this hybrid state for $\phi_A = 0.5000$ is higher than the free energy of either the lamellar form for $\phi_A = 0.4375$ or the cylindrical form for $\phi_A = 0.5625$. If true, this hypothesis would suggest that when $\phi_A = 0.5000$ a greater driving force in the underlayer is required to form the ML morphology instead of the well-aligned vertical lamellae morphology. This allows more preferential background regions to be utilized while still forming well-aligned vertical lamellae, as is the case for $\phi_A = 0.5000$ in Fig. 5. The more preferential background region drives down line defects that arise from poor guidance.

It should be noted that the measure of defectivity as used in the paper will give a higher measurement for the cylindrical ML morphology than for the lamellae ML morphology. This is because the lamellar ML morphology has a very well-formed vertical lamellae above the pinning stripe, whereas the cylindrical ML morphology does not. This can be seen in Fig. 5 when $n_{A,\text{background}} \to 0$ where the defectivity of $\phi_A = 0.4375$ is significantly lower than that of $\phi_A = 0.5625$.

These ML morphologies were found for a thin film ($t = 0.5 \cdot L_0$). Thicker films form different, more complex morphologies than these. While these thicker film morphologies are not explored in depth here, it will be shown in Sec. 3.6 that the transition volume fraction found for a thin film ($t = 0.5 \cdot L_0$) also shows improvement in the defectivity of a thicker film ($t = 0.75 \cdot L_0$). This suggests that while the transition volume fraction may change with film thickness, it is likely a minor change.

To summarize this section, the free energy of the ML morphology is dependent on the volume fraction of the BCP film. This allows the volume fraction to be tuned such that the ML will be less stable, allowing for more guidance in the system to decrease line defects without increasing morphological defects. For a symmetric BCP, the ideal volume fraction is found to be $\sim\phi_A = 0.5$.

3.6 *Density Asymmetry*

A BCP that has a mismatch in density is considered next. The ratio of densities in these BCPs is similar to that found in poly(styrene)-b-poly(methyl methacrylate). The results for various thicknesses of this BCP are shown in Fig. 7 for both density asymmetric cases, $\rho_A > \rho_B$ and $\rho_A < \rho_B$ (where the pinning stripe is always A). In both cases, it can be seen that films with a thickness of $0.75 \cdot L_0$ can form well-aligned vertical lamellae at lower background compositions due to the film thickness being incommensurate with the pitch. This is similar to how the symmetric BCP responded to thickness changes in Sec. 3.3. Because the dependence on film thickness is similar to the symmetric BCP (with the same CED for each block), the small difference in CED present in the density asymmetric BCPs is likely negligible in comparison to the difference in densities.

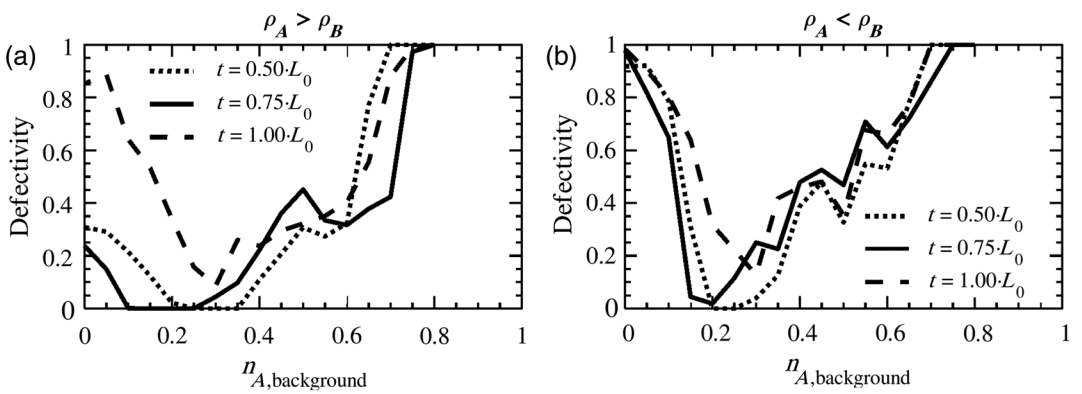

Fig. 7 Defectivity measurements of three different film thicknesses (t) for (a) a BCP with the density of block A greater than block B and (b) a BCP with the density of block A less than block B.

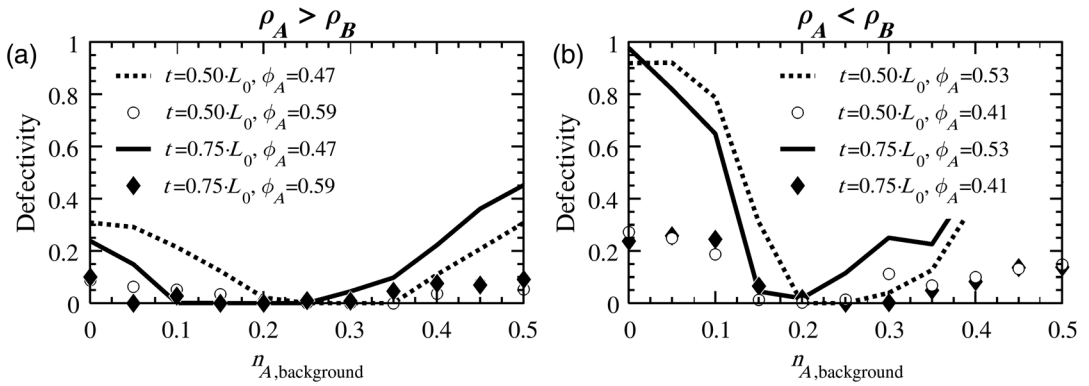

Fig. 8 Simulation results of (a) a BCP with the density of block A greater than block B and (b) a BCP with the density of block A less than block B. Volume fractions near $\phi_A = 0.5$ are shown by the solid and dashed lines while volume fractions near the transition between ML morphologies are shown by circles and diamonds.

When $n_{A,\text{background}} \to 0$, the defectivity of $\rho_A > \rho_B$ reaches far lower values than $\rho_A < \rho_B$. This is because $\rho_A > \rho_B$ forms the more lamellar form of the ML morphology, whereas $\rho_A < \rho_B$ forms the more cylindrical form as discussed in Sec. 3.5. The formation of the two different morphologies here is not driven by volume fraction, which is roughly 0.47 and 0.53 for $\rho_A > \rho_B$ and $\rho_A < \rho_B$, respectively. Rather, it is believed in this case to be driven by the difference in compressibilities of the two blocks, as shown in Table 1 for HPs 1 and 3. The half-cylinder morphology is preferred in the case where the B block is more compressible (higher density), whereas the half-lamellae morphology is preferred when the B block is less compressible. However, the opposite morphology can be formed by varying the volume fraction of the BCP.

In Sec. 3.5, it was shown that $\phi_A = 0.5$ is the composition for a symmetric BCP where the ML morphology transitions between the cylindrical and lamellar morphology, and it was hypothesized that this was the least stable ML morphology. For $\rho_A > \rho_B$ and $\rho_A < \rho_B$, this transition region is roughly at $\phi_A = 0.59$ and $\phi_A = 0.41$, respectively. The typical simulation series was run for both of these BCPs for both a film thickness of $t = 0.50 \cdot L_0$ and $t = 0.75 \cdot L_0$, the results of which are shown in Fig. 8. It can be seen that the change to the volume fraction did appear to improve the process window. The fact that a volume fraction that is greatly shifted away from $\phi_A = 0.5$, which was the ideal volume fraction in Fig. 5, improved the process helps support the proposed hypothesis. It is also worth noting that while this hypothesis was developed looking at thinner films ($t = 0.5 \cdot L_0$), it is remarkable that $t = 0.75 \cdot L_0$ films were also drastically improved by choosing this alternate film volume fraction. This suggests that this volume fraction is either independent or only weakly dependent on the thickness of the film. For both film thicknesses and both BCPs looked at here, the region where the defectivity measures as nonexistent appears to be wider. Additionally, when moving away from the defect-free vertical lamellae region, the defectivity increases at a slower rate. Near the ML morphology region this can be partially accounted for by the different morphology having a different base defectivity. However, it should be noted that the defectivity also increases at a slower rate in the poorly aligned lamellae region. As discussed in Sec. 3.5 for a BCP that did not have a density mismatch, having a volume fraction other than $\phi_A = 0.5$ appears to increase chain jumping, which likely results in faster kinetics of defect annihilation.

4 Conclusions

A coarse-grained molecular dynamics model was used to explore how various BCPs self-assemble on various guiding underlayers. It was found that as the background region composition is varied in the underlayer, films go through four primary morphologies: ML, well-aligned vertical lamellae, poorly aligned vertical lamellae, and horizontal lamellae. Furthermore, there appears to be two different forms of ML morphology for thin films ($t = 0.50 \cdot L_0$), a cylindrical form and a lamellar form. Two forms of defectivity are discussed: line defects (dislocations, jogs, etc.) in vertical lamellae, and morphological defects (transitioning to an incorrect morphology such as ML or horizontal lamellae). Line defectivity decreases with increasing contrast between the pinning stripe and the background region, whereas morphological defects occur at extremes in background region preference. This suggests the ideal case is having as preferential a background region as possible without forming morphological defects. The film is found to be fairly insensitive to minor variations in the width of the pinning stripe, though significantly oversizing the pinning stripe increases defectivity.

A frustrated film thickness is found to give a larger window for forming well-aligned vertical lamellae for symmetric BCPs and density asymmetric BCPs. When there is a CED asymmetry in the BCP, film thickness has a large effect on the optimal background region composition for forming well-aligned vertical lamellae. The best-case scenario found with regard to the size of the process window is using a CED asymmetric BCP with a pinning stripe that is composed of the lower CED block. This allows lower composition background regions to be used before forming the ML morphology, which increases the guidance of the system.

Shifting the volume fraction of a symmetric or density asymmetric BCP away from $\phi_A = 0.5$ extends the well-aligned vertical lamellae regime to more neutral background region compositions. It is theorized this is due to an increase in defect annihilation kinetics due to bridge formation in the

film being easier. For a symmetric BCP, shifting the volume fraction away from $\phi_A = 0.5$ causes the ML morphology to occur at higher background region compositions. It is hypothesized that this is due to $\phi_A = 0.5$ being the composition where the ML morphology transitions between the cylindrical and lamellar morphology, making it the least stable ML morphology. At this transition, more preferential background regions are required to form the ML morphology, allowing the lower background compositions to be reached while remaining in the well-aligned vertical lamellae region. The same phenomenon is observed for the density asymmetric BCP, though a different volume fraction is required due to the asymmetry in the compressibilities of the blocks. The transition volume fraction was determined from a thin film simulation ($t = 0.5 \cdot L_0$), though the same transition volume improved the process window of a thicker film ($t = 0.75 \cdot L_0$). This suggests the transition volume fraction is only minorly affected, if at all, by the film thickness, though more work is needed to confirm this.

Acknowledgments

Intel for funding the purchase of the computer cluster used for this work. This material was based upon work supported by the National Science Foundation under Grant Nos. CMMI-1534461 and CBET-1512517. Any opinions, findings, and conclusions or recommendations expressed in this material are those of the author(s) and do not necessarily reflect the views of the National Science Foundation.

References

1. M. W. Matsen and F. S. Bates, "Unifying weak- and strong-segregation block copolymer theories," *Macromolecules* **29**, 1091–1098 (1996).
2. L. Leibler, "Theory of microphase separation in block copolymers," *Macromolecules* **13**, 1602–1617 (1980).
3. F. S. Bates and G. H. Fredrickson, "Block copolymer thermodynamics: theory and experiment," *Annu. Rev. Phys. Chem.* **41**, 525–557 (1990).
4. R. A. Lawson et al., "Effect of χN and underlayer composition on self-assembly of thin films of block copolymers with energy asymmetric block," *Proc. SPIE* **9423**, 94231L (2015).
5. A. J. Peters et al., "Detailed molecular dynamics studies of block copolymer directed self-assembly: Effect of guiding layer properties," *J. Vac. Sci. Technol. B* **31**, 06F302 (2013).
6. F. A. Detcheverry et al., "Interpolation in the directed assembly of block copolymers on nanopatterned substrates: simulation and experiments," *Macromolecules* **43**(7), 3446–3454 (2010).
7. C. Liu et al., "Chemical patterns for directed self-assembly of lamellae-forming block copolymers with density multiplication of features," *Macromolecules* **46**, 1415–1424 (2013).
8. F. A. Detcheverry et al., "Simulations of theoretically informed coarse grain models of polymeric systems," *Faraday Discuss.* **144**, 111–125 (2010).
9. B. D. Nation et al., "Predicting process windows for pattern density multiplication using block copolymer directed self-assembly in conjunction with chemoepitaxial guiding layers," *Proc. SPIE* **9049**, 90491C (2014).
10. R. A. Lawson et al., "Coarse grained molecular dynamics model of block copolymer directed self-assembly," *Proc. SPIE* **8680**, 86801Y (2013).
11. C. Sinturel, F. S. Bates, and M. A. Hillmyer, "High χ low N block polymers: How far can we go?," *ACS Macro Lett.* **4**(9), 1044–1050 (2015).
12. MATLAB version 8.0.0.783, The MathWorks Inc., Matick, Massachusetts (2015).
13. "HOOMD-blue web page," (2015), http://codeblue.umich.edu/hoomd-blue.
14. J. A. Anderson, C. D. Lorenz, and A. Travesset, "General purpose molecular dynamics simulations fully implemented on graphics processing units," *J. Comput. Phys.* **227**, 5342–5359 (2008).
15. A. J. Peters et al., "Coarse-grained molecular dynamics modeling of the kinetics of lamellar block copolymer defect annealing," *J. Micro/Nanolithogr. MEMS MOEMS* **15**(1), 013508 (2016).

Benjamin D. Nation completed his BSc(Hons) degree in chemical engineering at Tennessee Technological University in 2012. He is a PhD candidate at the Georgia Institute of Technology under the advisement of Professors Clifford L. Henderson and Peter J. Ludovice at the Georgia Institute of Technology. His research is on the simulation of BCP directed self-assembly.

Peter J. Ludovice is an associate professor of chemical engineering at the Georgia Institute of Technology. After completing his BS and PhD degrees in chemical engineering from the University of Illinois and M.I.T., respectively, he carried out molecular modeling research at the ETH-Zürich, IBM, NASA, and Molecular Simulations Inc., (now BIOVIA). His current research focuses on the computer simulation of synthetic and biological macromolecules.

Clifford L. Henderson is a professor in the School of Chemical and Biomolecular Engineering at the Georgia Institute of Technology and an adjunct professor in the School of Chemistry and Biochemistry at Georgia Tech. He received his BSc degree in chemical engineering with highest honors from Georgia Institute of Technology and his MSc and PhD degrees in chemical engineering from the University of Texas at Austin.